

Computer-aided diagnosis of dysplasia in Barrett's esophagus using endoscopic optical coherence tomography

Xin Qi

Case Western Reserve University
Department of Biomedical Engineering
Cleveland, Ohio 44106

Michael V. Sivak Jr.

Gerard Isenberg
Case Western Reserve University
Department of Medicine
Cleveland, Ohio 44106

Joseph. E. Willis

Case Western Reserve University
Department of Pathology
Cleveland, Ohio 44106

Andrew M. Rollins

Case Western Reserve University
Department of Biomedical Engineering
and Department of Medicine
Cleveland, Ohio 44106
E-mail: rollins@case.edu

Abstract. Barrett's esophagus (BE) and associated adenocarcinoma have emerged as a major health care problem over the last two decades. Because of the widespread use of endoscopy, BE is being recognized increasingly in all Western countries. In clinical trials of endoscopic optical coherence tomography (EOCT), we defined certain image features that appear to be characteristic of precancerous (dysplastic) mucosa: decreased scattering and disorganization in the microscopic morphology. The objective of the present work is to develop computer-aided diagnosis (CAD) algorithms that aid the detection of dysplasia in BE. The image dataset used in the present study was derived from a total of 405 EOCT images (13 patients) that were paired with highly correlated histologic sections of corresponding biopsies. Of these, 106 images were included in the study. The CAD algorithm used was based on a standard texture analysis method (center-symmetric auto-correlation). Using histology as the reference standard, this CAD algorithm had a sensitivity of 82%, specificity of 74%, and accuracy of 83%. CAD has the potential to quantify and standardize the diagnosis of dysplasia and allows high throughput image evaluation for EOCT screening applications. With further refinements, CAD could also improve the accuracy of EOCT identification of dysplasia in BE. © 2006 Society of Photo-Optical Instrumentation Engineers. [DOI: 10.1117/1.2337314]

Keywords: Barrett's esophagus; dysplasia; endoscopic optical coherence tomography; computer-aided diagnosis.

Paper 06006R received Jan. 13, 2006; revised manuscript received Apr. 11, 2006; accepted for publication Apr. 11, 2006; published online Aug. 28, 2006. This paper is a revision of a paper presented at the SPIE conference on Coherence Domain Optical Methods and Optical Coherence Tomography in Biomedicine VIII, Jan. 2004, San Jose, California. The paper presented there appears unrefereed in SPIE Proceedings Vol. 5316.

1 Introduction

Barrett's esophagus (BE) is an acquired condition, thought to be due to gastroesophageal reflux, in which the normal stratified squamous epithelium is replaced by a columnar-type epithelium in which specialized intestinal metaplasia occurs. BE is being recognized increasingly in all Western countries as the use of endoscopy becomes widespread. BE and associated adenocarcinoma have emerged as a major health care problem.¹⁻⁴ Adenocarcinoma is thought to develop as a sequence of transformations, from the nondysplastic columnar Barrett's epithelium, through low-grade and high-grade dysplasia and finally invasive cancer.⁵⁻⁸ A 30-40-fold increase in the incidence of esophageal adenocarcinoma has been demonstrated in patients with BE.^{1,4,9}

Although BE is readily diagnosed during a standard endoscopic examination, it is extremely difficult endoscopically to

identify the presence of low-grade dysplasia (early precancerous tissue transformation) within a segment of Barrett's epithelium. Thus, current clinical management for patients with BE includes periodic endoscopic examinations with multiple biopsies being obtained according to a standard protocol, specifically four-quadrant biopsies obtained with a large forceps at 2-cm intervals along the length of the Barrett's epithelium, the so-called Seattle protocol.¹⁰ If dysplasia is detected microscopically, monitoring procedures are repeated more frequently, generally every 6 months for low-grade dysplasia and 3 months for high-grade dysplasia. If repeat tissue sampling reveals high-grade dysplasia, particularly if found in several of the biopsies, further intervention is usually recommended.¹¹⁻¹³ However, the major limitation of this approach to management is sampling error.¹⁰ By definition, BE must involve at least 2 cm of the length of the distal esophagus, but typically it involves much longer segments, occasionally the entire length of the esophagus. Even with rigorous adherence to the biopsy protocol, only a tiny fraction of the

Address all correspondence to Andrew Rollins, Biomedical Engineering, Case Western Reserve University, 10900 Euclid Ave., Cleveland, OH 44106-7207 United States of America; Tel: 216 368 1917; Fax: 216 368 0847; E-mail: rollins@case.edu

entire surface area of the involved esophagus is sampled. Moreover, the pattern of dysplasia within Barrett's epithelium is always irregular with foci that range from tiny to large.

Optical coherence tomography (OCT) is an emerging optical technique based on low-coherence interferometry that provides noninvasive, subsurface, high-resolution imaging of biological microstructure.^{14,15} Endoscopic OCT (EOCT) has been enabled by the development of fiber-optic catheter probes that can be inserted through standard endoscopes.¹⁵⁻¹⁹ EOCT differentiates the tissue layers of the gastrointestinal (GI) wall and can identify dysplasia with the mucosa.²⁰⁻²² In theory, EOCT could be used in BE to target biopsies to mucosal sites where the probability for the presence of dysplasia is high.^{18,20,23-25} In the future, if sufficient sensitivity is achieved, EOCT could decrease sampling error and increase yield; ultimately it could even eliminate the need for tissue sampling.

We developed a real-time EOCT imaging system¹⁶ and have gained experience with this imaging method in a series of clinical trials.^{21-23,25-27} Our EOCT system is based on a high-speed OCT engine described elsewhere.²⁸ The EOCT catheter probe is introduced into the GI tract through the accessory channel of a standard endoscope. The OCT light exits the catheter probe near the tip in a radial fashion and is focused approximately 2.5 mm from the probe surface with a minimum spot diameter of approximately 25 μ . The focused light exiting the probe tip sweeps a circular pattern as the internal optics rotate at four revolutions per second.¹⁶

We and others have demonstrated that EOCT is feasible in the human GI tract and that it provides interpretable, high-resolution images of the mucosa and submucosa.^{21,23,26,27,29} The EOCT catheter probe is analogous to catheter ultrasound probes that are commercially available for endoscopic imaging. We therefore compared the performance of our EOCT probe to catheter probe endoscopic ultrasonography (CPEUS) *in vitro* and *in vivo* and found that the former provided superior resolution, but with limited depth of penetration such that imaging was limited to the mucosa and submucosa.²⁶ Additionally, EOCT differentiated major structures within mucosa and submucosa whereas CPEUS did not. In another clinical study, we demonstrated that EOCT differentiated adenomatous from hyperplastic polyps and normal colon tissue.²¹ Because the adenomatous polyp is essentially a form of dysplasia, this study also confirmed our hypothesis with regard to the EOCT characteristics of dysplastic mucosa, i.e., a decreased scattering signal and loss of the structure associated with normal histological organization. These characteristics features are also present in EOCT images of BE with dysplasia.^{18,23,25} Figure 1 shows examples of EOCT images of nondysplastic BE (A), low-grade dysplasia in BE (B), high-grade dysplasia in BE (C), and adenocarcinoma (D).

In general, computer-aided diagnosis (CAD) systems identify lesions in medical images by extracting quantitative features and identifying anomalies by comparisons with known features of images of normal and diseased tissue. CAD is useful because it can provide an objective, quantitative interpretation of clinical images, a type of "second opinion" the physician can use to guide diagnosis and therapy.^{30,31} CAD techniques could enhance the effort to identify dysplasia in BE in at least three ways: first, CAD could quantify and standardize the identification of image characteristics associated

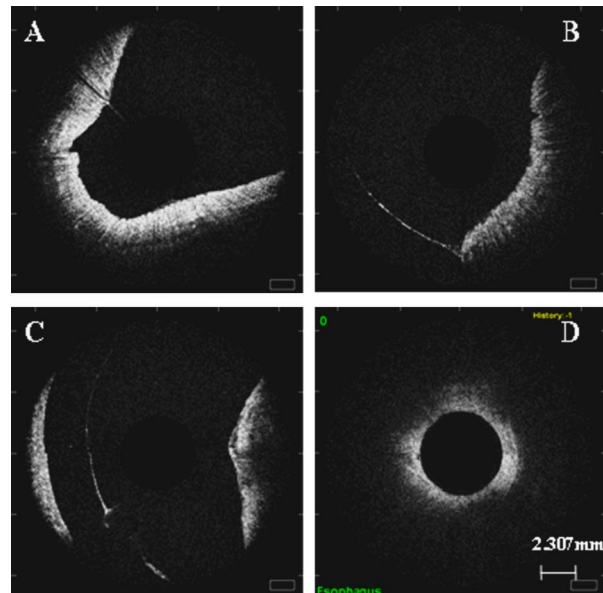


Fig. 1 EOCT images of Barrett's esophagus (A), low-grade dysplasia (B), high-grade dysplasia (C), and adenocarcinoma (D).

with dysplasia, and thereby reduce inter-observer and intra-observer variability. Second, the use of EOCT as a surveillance modality for fully developed BE^{23,25} would yield thousands of images for a single patient. It is improbable that a human reader (endoscopists) could accurately evaluate such a large dataset within a reasonable time frame, certainly not in real time. EOCT surveillance would be a repetitive, tiresome process involving mostly images of nondysplastic Barrett's epithelium. CAD is ideally suited to this type of task.³¹ Third, it is possible that CAD could improve the accuracy of identification of dysplasia in EOCT images of BE, although this would not be essential to the realization of the first two goals.

EOCT readily distinguishes Barrett's esophagus from normal esophageal mucosa,^{17,18,23,29} but the identification of dysplasia within Barrett's epithelium is more challenging. Using the image features that we have defined as characteristic of dysplasia, a prospective study was conducted to test the ability of endoscopists to diagnose dysplasia in BE. Although the results were encouraging, the overall accuracy of EOCT (78%) obtained to date has been insufficient with respect to making clinical decisions. Moreover, significant inter-observer variability and intra-observer variability was noted.²⁵ Therefore, we tested the feasibility of CAD as a way to improve the accuracy and usefulness of EOCT in the diagnosis of dysplasia in BE.

2 Materials and Methods

Under a protocol approved by the Institutional Review Board of University Hospitals of Cleveland, we are investigating the role of EOCT during surveillance endoscopy in patients with BE. The protocol specifies that surveillance be conducted according to the standard "Seattle protocol,"¹⁰ with biopsies being obtained in four quadrants at 2-cm intervals along the entire length of esophagus involved by Barrett's changes. A digital stream of EOCT images is obtained at each biopsy site prior to removal of the actual biopsy. For this purpose, a 2.4-

mm-diameter EOCT probe was designed for use with a cap-fitted, 2-channel endoscope (Olympus models GIF 2T 160 and GIF 2T 240).

The cap, a transparent, plastic cylinder beveled at the distal end, fits tightly on the end of the endoscope. When the tip of the endoscope is deflected toward the wall of the esophagus, a small circular portion of the esophageal mucosa is fixed by the cap, thereby negating the effects of esophageal motion. With the EOCT probe inserted through one of the two accessory channels in the endoscope, a portion of the esophageal mucosa within the area encircled by the cap is imaged. To accomplish this, it was necessary to offset the imaging plane of the probe 30 degrees from perpendicular and to set the focal point at 3 mm. As a digital stream of images is being obtained, a biopsy forceps inserted through the second endoscope channel is used to obtain a specimen. The endoscope has a mechanism at the distal port of the second channel that can be used to deflect an accessory inserted through the channel. When the cap is properly aligned on the tip of the endoscope, the lever mechanism is used to deflect the biopsy forceps into the EOCT imaging field. Thus, a biopsy can be taken from exactly the same region of mucosa that is being imaged by EOCT. In fact, removal of the biopsy results in a divot in the mucosa that is readily evident in the EOCT image. Using this system, EOCT images can be precisely correlated to the histopathologic features of the mucosa.

In this study, an experienced GI pathologist, blinded to endoscopic and EOCT findings, evaluated each biopsy using standard criteria. The histopathological findings were classified as no dysplasia, indefinite for dysplasia, low-grade dysplasia, high-grade dysplasia, and intramucosal cancer. The endoscopic procedures were performed by one of four endoscopists in patients with known Barrett's esophagus who were undergoing surveillance endoscopy (some had dysplasia in biopsies obtained at prior examinations). Each endoscopist separately reviewed the EOCT digital image stream after the procedure and rated EOCT findings according to the presence or absence of dysplasia. A total of 314 EOCT image streams paired with biopsy diagnoses from 33 patients were analyzed in the study. Using the pathologist's diagnosis as the standard, the performance of EOCT was sensitivity, 68%; specificity, 82%; positive predictive value, 53%; negative predictive value, 89%; and diagnostic accuracy, 78%. Diagnostic accuracy for the four endoscopists ranged from 56% to 98%. The results of this study are reported elsewhere.²⁵

For the present study, an image database was constructed of image-biopsy pairs obtained during endoscopic surveillance procedures in 13 patients. An EOCT image stream (approximately 20 frames) was recorded at each biopsy site. One EOCT image from the stream was selected for analysis. The image selected was the last image recorded immediately before the biopsy forceps entered the EOCT field of view. For each biopsy site, all EOCT image streams were reviewed jointly by two investigators (XQ, MVS). Each biopsy was evaluated by an experienced GI pathologist (JEW). The image-biopsy pair selection criteria were as follows: (1) entry of the biopsy forceps into the EOCT imaging field had to be clearly visible to insure perfect image-biopsy correlation; (2) an EOCT image of good quality, without distortion or artifact; (3) the biopsy was interpreted as nondysplastic BE or as low- or high-grade dysplasia (i.e., biopsies graded as indefinite for

dysplasia or as cancer were excluded). Of a total of 405 image-biopsy pairs collected, 106 met inclusion criteria: 68 graded as nondysplastic, 38 graded as dysplastic.³²

CAD processing was implemented in three phases: the first is segmentation of the region of interest (ROI) in EOCT images. The ROI in an EOCT image is the tissue that was removed as the biopsy; nontissue image features, such as the cap, and sometimes tissue outside the cap are excluded. The ROI is the only portion of the EOCT image subjected to the second phase, feature extraction. Based on our clinical observation of decreased tissue organization in dysplastic versus normal or benign mucosa, image texture analysis was selected as the feature extraction method. In EOCT images of BE, a decrease in tissue organizational structure appears as a more homogenous texture, which can be quantified using texture analysis. Texture features that can be quantified include measures of smoothness, coarseness, and regularity.³³ The third phase is tissue classification. Texture features are input to a statistical model, called a classifier, which groups the images as dysplastic or nondysplastic tissue. Leave-one-out cross-validation and the receiver operating characteristic (ROC) curve were used to evaluate the performance of CAD.

2.1 Segmentation Methods

For the purposes of this study, a semi-automatic segmentation process was developed. The cap and tissue outside the cap were deleted manually from the image. Global thresholding was used, based on the assumption that the image has a bimodal histogram, to obtain a binary image. The binary image was multiplied with the original filtered image to remove the background noise, resulting in a clean EOCT image without background noise and cap artifacts. Edge detection and morphological processing yielded a continuous and smooth region of interest (ROI) corresponding to the tissue under examination. First, the intensity of image was rescaled to cover the entire dynamic range, which can increase the contrast of output image. The Sobel kernel was used to find edges of the image via the Sobel approximation to the derivative. The edges at those points are the maximum of their gradients. The threshold for Sobel method is half of global image threshold using Otsu's method.³⁴ We used morphological processing to dilate the binary image with line structuring elements at 0 degrees and 90 degrees, then erode it with a "rolling ball" disk structuring element to smooth the edges.³⁵ Finally, a binary mask defining the ROI was produced, which was used for the next step, feature extraction.

2.2 Feature Extraction Methods

Texture analysis is a class of image processing techniques designed to quantify image properties such as smoothness, coarseness, and regularity.³⁶⁻³⁹ By clinical experience, we have observed certain characteristics of EOCT images that correlate with dysplastic mucosa in Barrett's esophagus, including decreased scattering signal and loss of structure associated with normal histological organization.^{18,23,25} The EOCT images do not contain such texture structures as large-scale replications, symmetries, or combinations of various basic patterns. Because the EOCT intensity and structural image features tend to vary locally, we chose the center-symmetric



Fig. 2 3×3 neighborhood of pixels with 4 center-symmetric pairs (g_i and g'_i , here $i=1, 2, 3, 4$), used to compute CSAC measures. Here, g_i and g'_i are the intensity values of the center-symmetric pair.

auto-correlation (CSAC) method for this study. The CSAC texture features relate to local intensity variations and can capture local structure variation.

CSAC is a texture analysis method that quantifies the relationships between each pixel and its neighboring pixels.⁴⁰ In our study, for each image, six CSAC measures were calculated: gray-scale texture covariance (SCOV); local variance (VAR); between-pair variance (BVAR); within-pair variance (WVAR); variance ratio (SVR); and normalized SCOV (SAC). A mathematical description of these measures calculated for center-symmetric pairs of pixels in a 3×3 neighborhood (as shown in Fig. 2) are presented in Eqs. (1)–(6). Table 1 defines these abbreviations.

$$SCOV = \frac{1}{4} \sum_i^4 (g_i - \mu)(g'_i - \mu) \quad (1)$$

$$VAR = \left[\frac{1}{8} \sum_i^4 (g_i^2 + g_i'^2) \right] - \mu^2 \quad (2)$$

$$BVAR = \left[\frac{1}{16} \sum_i^4 (g_i + g_i')^2 \right] - \mu^2 \quad (3)$$

Table 1 Abbreviations of image analysis measures.

CSAC	Center-symmetric autocorrelation
SCOV	Gray level texture covariance
VAR	Local variance
BVAR	Between-pair variance
WVAR	Within-pair variance
SVR	Variance ratio
SAC	Normalized SCOV

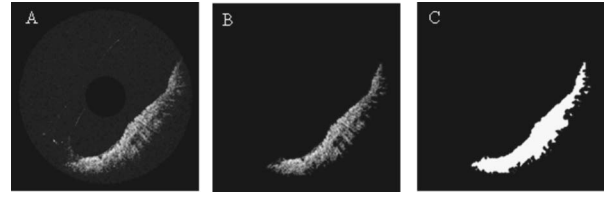


Fig. 3 EOC image of Barrett's esophagus (A); region of interest (ROI) without background noise and cap artifacts (B); binary mask defining the ROI.

$$WVAR = \frac{1}{16} \sum_i^4 (g_i - g_i')^2 \quad (4)$$

$$SVR = \frac{WVAR}{BVAR} \quad (5)$$

$$SAC = \frac{SCOV}{VAR} \quad (6)$$

where g_i refers to the gray level of pixel i , here $i=1, 2, 3, 4$ and μ denotes the local mean value.

SCOV is a measure of the pattern correlation as well as the local pattern contrast. VAR is a measure of local gray-level variation and is the sum of BVAR and WVAR. BVAR is a measure of between-pair intensity variance. WVAR is a measure of within-pair intensity variance. SVR, the symmetric variance ratio between the within-pair and between-pair variances, is a statistic equivalent to the auto-correlation measure SAC. SAC is a normalized gray-level invariant version of the texture covariance measure SCOV. It is invariant under linear gray-level shifts such as correction by mean and standard deviation.⁴⁰

2.3 Classification Methods

Principal component analysis (PCA) is used to reduce the dimensionality of a dataset that consists of a large number of interrelated variables, while retaining as much as possible of the variation present in the dataset.⁴¹ Each principal component is a linear combination of the original variables. The first few principal components typically contain most of the variance present in all of the original data. For this study the six texture features were calculated for every EOC image in the dataset and evaluated as classifiers. Then, PCA was carried out and the first two principal components (pc1 and pc2) were evaluated as classifiers. Using the pathologist's diagnosis of each biopsy as the reference standard, two methods were used to evaluate the performance of the CAD algorithm and the value of six texture features and pc1 and pc2 as classifiers.

First, the receiver operating characteristic (ROC) curve was generated for those variables and the areas under the curves were calculated. Second, due to the limitation in sample size (106 images), a statistical re-sampling technique called leave-one-out cross-validation was used to estimate the sensitivity, specificity, positive predictive value (PPV), negative predictive value (NPV), and accuracy of those variables

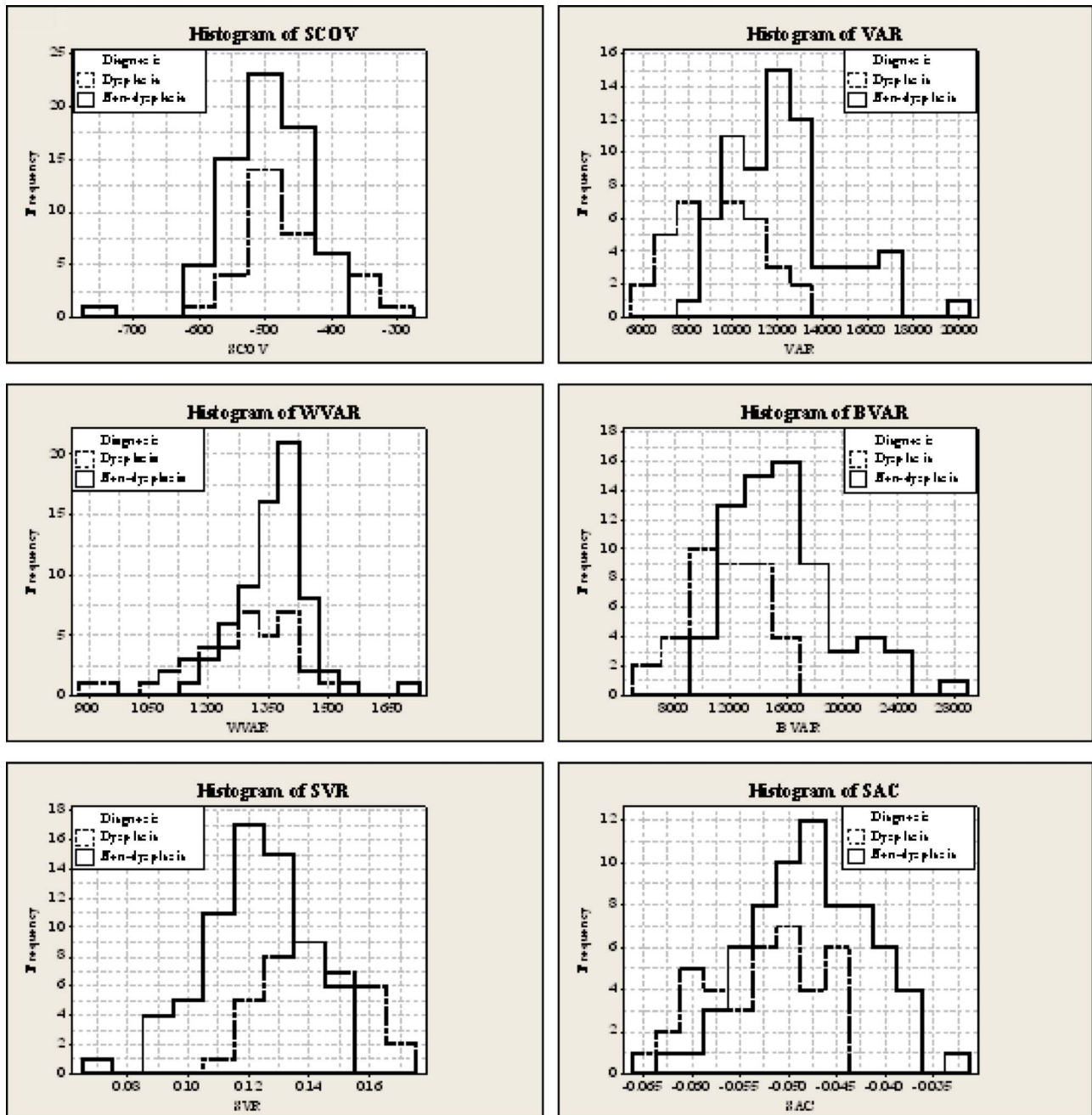


Fig. 4 The histograms of six CSAC texture features within the ROI extracted from 68 nondysplastic Barrett's and 38 dysplastic EOCT images.

as classifiers.⁴² For this, the maximum accuracy point (minimum sum of false negative and false positive) was used as the decision threshold.

3 Results

3.1 Segmentation Results

All 106 EOCT images included in this study were successfully segmented in order to identify the region of interest representing the tissue from which the biopsy was obtained. Figure 3 illustrates the segmentation process using a representative EOCT image (non-dysplastic). In Fig. 3(A), background noise and the plastic cap are evident. The cap was

removed manually from the image. Using global thresholding and filtering, as mentioned in the materials and method section on segmentation methods, a clean EOCT image without background noise and cap artifact was obtained, as shown in Fig. 3(B).

Using edge detection and morphological processing, as mentioned in the materials and method section on segmentation, a binary mask defining the ROI was obtained, as shown in Fig. 3(C). Within the next phase, Fig. 3(B) is processed to extract texture features within the area defined by its binary mask (Fig. 3(C)).

Table 2 Numerical comparison of ROC curves for each feature of CSAC.

TCH	Area under ROC (95% CI)	Sensitivity (95% CI)	Specificity (95% CI)	Positive predictive value (95% CI)	Negative predictive value (95% CI)	Diagnostic accuracy (95% CI)
SCOV	67% (57%~75%)	50% (35%~65%)	82% (72%~90%)	61% (44%~76%)	75% (64%~83%)	71% (62%~89%)
VAR	83% (75%~90%)	82% (66%~91%)	74% (62%~83%)	63% (49%~75%)	88% (77%~94%)	76% (67%~84%)
BVAR	84% (75%~90%)	87% (72%~95%)	69% (57%~79%)	61% (48%~73%)	90% (79%~96%)	75% (66%~83%)
WVAR	70% (61%~79%)	61% (45%~75%)	74% (62%~83%)	56% (41%~70%)	77% (65%~86%)	69% (60%~77%)
SVR	80% (72%~88%)	74% (58%~85%)	74% (62%~83%)	61% (47%~74%)	83% (72%~91%)	74% (64%~81%)
SAC	71% (62%~80%)	82% (66%~91%)	52% (40%~63%)	48% (37%~60%)	83% (69%~92%)	62% (53%~71%)

3.2 Feature Extraction Results

Using the center-symmetric auto-correlation method, texture covariance (SCOV), normalized texture covariance (SAC), variance ratio (SVR), local variance (VAR), between-pair variance (BVAR), and within-pair variance (WVAR) were calculated over the ROI segmented in each of the 106 EOCT images. Figure 4 shows the histograms of those six CSAC features within the ROI in EOCT images. Here we group the 106 EOCT images into two groups: 68 images of nondysplastic mucosa and 38 of dysplastic mucosa (31 low-grade dysplasia, 7 high-grade dysplasia).

3.3 Classification Results

In this study, the first two principal components captured 94% of the variation present in the six texture features. The histograms of the scores of the first two principal components are shown in Fig. 5.

The ROC curves for each texture feature from the CSAC calculations are shown in Fig. 6. Table 2 gives the area under

each ROC curve. Also shown in Table 2 are the sensitivity, specificity, PPV, NPV, and diagnostic accuracy calculated by leave-one-out cross-validation.

The ROC curves for the first and second principal components calculated from the six texture features are shown in Fig. 7. Table 3 shows the area under ROC curve and the sensitivity, specificity, PPV, NPV, and diagnostic accuracy for pc1 and pc2.

4 Discussion

From Table 2, local intensity variation (VAR) and between-pair intensity variation (BVAR) are the most important texture features for classification of nondysplasia and dysplasia in EOCT images of BE. They achieved essentially the same area under the ROC (75% ~ 90% CI). This is because VAR is the sum of BVAR and WVAR, and BVAR occupies most of VAR. From Table 3, although the PCA did not improve the diagnostic accuracy, compared with the most important texture features (VAR and BVAR), the pc1 and pc2 gave the same clas-

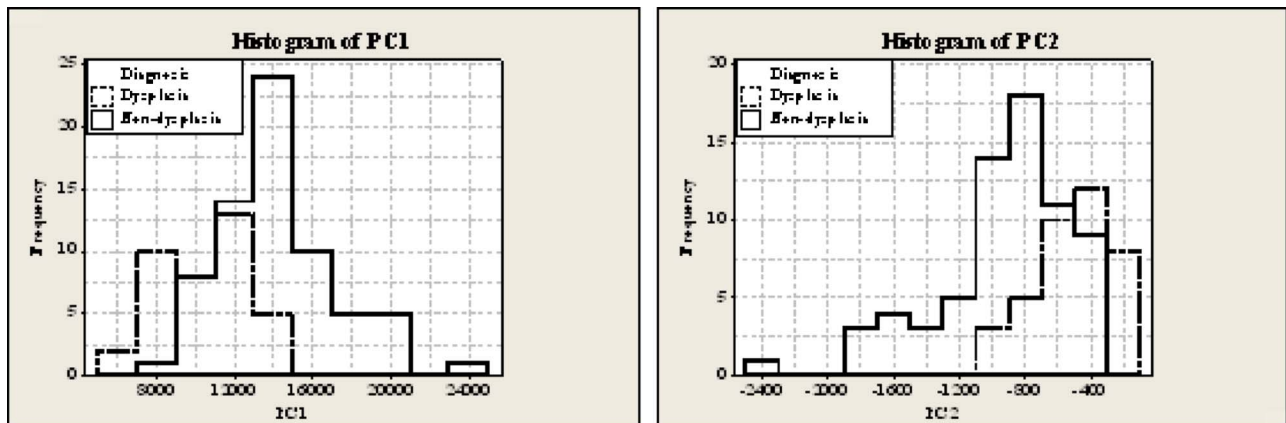


Fig. 5 The histograms of first two principal components (PC1 and PC2) for nondysplastic images and dysplastic images.

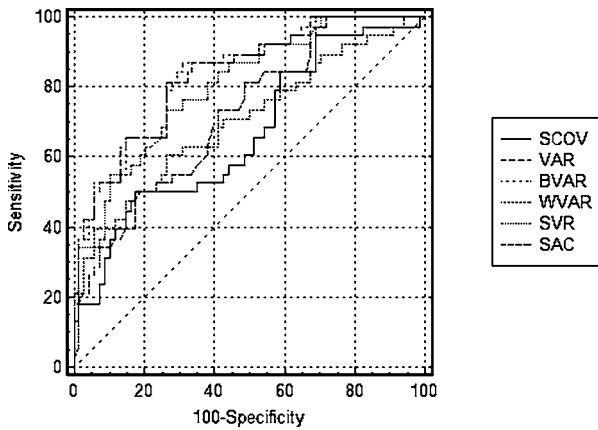


Fig. 6 The graphic comparison of ROC curves for each feature of CSAC.

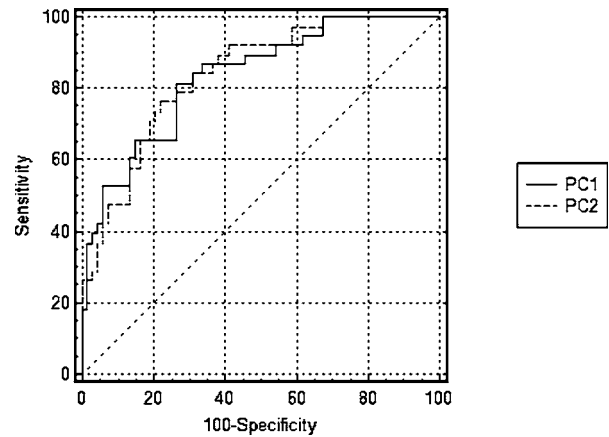


Fig. 7 The graphic comparison of ROC curves for the first and second principal components of six features of CSAC.

sification result (area under ROC) as VAR and BVAR. Because VAR and BVAR, of the 6 texture features, captured most of the variance of the dataset, pc1 and pc2 should have the same axes as VAR and BVAR. For the present study, only a single image per biopsy site was used. PCA did not improve the classification. However, in the future PCA may be useful for feature classification where multiple images per biopsy site are obtained.

Due to beam focusing and a radial scanning geometry, the EOCT does not sample the tissue space uniformly. Signals returned from the beam focus sample smaller tissue volumes than signals away from the beam focus. Sample spacing is closer near to the probe and farther apart away from the probe. We did not perform any test to determine the effects of the nonuniform sampling on the CAD procedure. However, due to the controlled manner in which the images were acquired, the region of interest in each image was located approximately the same distance from the probe. Therefore, we expect any effects of nonuniform sampling to be minimal in this study.

In the previous study, the EOCT system with human readers has an accuracy of 78% for detection of dysplasia in patients with Barrett's esophagus.²⁵ These data are reproduced in Table 4. However, image selection criteria for CAD were much stricter than those employed by the endoscopists. For each image and biopsy pair used in the present study, there was a high degree of certitude that the biopsy forceps entered the EOCT field of view, thereby ensuring nearly perfect

image-biopsy correlation. Of a total of 405 image-biopsy pairs collected by endoscopists, 106 met inclusion criteria for the present study. On the other hand, the endoscopists grading the images had access to the real-time image stream consisting of many images at each biopsy site, while the CAD algorithm analyzed only one image per biopsy site. Because of these differences, the results of the CAD grading must be compared cautiously with the previously reported grading by endoscopists. However, from the results it appears that CAD is at least as accurate as humans for identification of dysplasia in EOCT images.

In a study that included 121 patients with BE, Poneros et al. found that OCT can reliably distinguish squamous epithelium from normal gastric mucosa.⁴³ A later study that included 109 biopsy-correlated images from 46 patients with BE found the sensitivity and specificity of EOCT (one blinded investigator) to be, respectively, 68% and 70% for classification of nondysplasia versus dysplasia (including low-grade, high-grade, and indeterminate).⁴⁴ These results are comparable to those of our previous study of EOCT for the detection of dysplasia in BE (68% sensitivity, 82% specificity). Jackle et al. found that EOCT images of BE differed substantially from those of normal esophagus, reflux esophagitis, and esophageal carcinoma.⁴⁵

Other optical modalities, in addition to EOCT, have been employed for the detection of dysplasia in BE. Some of these techniques use diagnostic molecular and microstructural information contained in light-tissue interactions such as fluo-

Table 3 Numerical comparison of ROC curves for the first and second principal components of six features of CSAC.

	Area under ROC (95% CI)	Sensitivity (95% CI)	Specificity (95% CI)	Positive predictive value (95% CI)	Negative predictive value (95% CI)	Diagnostic accuracy (95% CI)
PC1	83% (75%~90%)	82% (66%~91%)	74% (62%~83%)	63% (49%~75%)	88% (77%~94%)	76% (67%~84%)
PC2	84% (75%~90%)	76% (61%~87%)	78% (67%~86%)	66% (51%~78%)	85% (75%~92%)	77% (69%~84%)

Table 4 Evaluation of EOCT classification by endoscopists.

Sensitivity	68% (56% ~ 77%)
Specificity	82% (76% ~ 86%)
Positive predictive value	53% (43% ~ 63%)
Negative predictive value	89% (84% ~ 93%)
Diagnostic accuracy	78% (73% ~ 83%)

Total of 314 imaging biopsy sites (95% confidence interval)
From Isenberg et al.

rescence, light scattering, and Raman scattering. Using 97 quantitative fluorescence spectra obtained from 20 patients, Brand et al. distinguished high-grade dysplasia from nondysplastic tissue types with 77% sensitivity and 71% specificity.⁴⁶ Light-scattering spectroscopy can be used to measure epithelial nuclear enlargement and crowding. Using this technique, Wallace et al. studied 13 patients with BE (76 sites: 4 high-grade dysplasia, 8 low-grade dysplasia, 12 indefinite for dysplasia, and 52 nondysplastic Barrett's from 13 Barrett's patients.) Dysplasia was considered to be present if more than 30% of the nuclei were enlarged ($>10 \mu\text{m}$ as threshold diameter). The reported sensitivity and specificity for detecting dysplasia (either low-grade or high-grade) were, respectively, 90% and 90%.⁴⁷ In a study reported by Wong et al., Raman spectroscopy differentiated high-grade dysplasia from nondysplastic Barrett's epithelium and low-grade dysplasia with an 88% sensitivity and 89% specificity.⁴⁸ These optical spectroscopy techniques provide single "point" measurements obtained with a probe, whereas EOCT provides real-time digital images that are highly correlated with the histopathologic morphology of the esophageal wall. Thus, EOCT may be better suited for clinical screening and surveillance procedures and is easier for physicians to review.

Nonoptical techniques have also been used to evaluate BE. Endoscopic ultrasound (EUS) appears to have a role in patients who have BE and high-grade dysplasia or intramucosal carcinoma, in whom a nonoperative therapy is being contemplated. In most cases, however, EUS is incapable of detecting low-grade and high-grade dysplasia.⁴⁹ Chromoendoscopy and magnification endoscopy are endoscopic techniques, sometimes used together, that improve visualization of the surface of the gastrointestinal mucosa. They are potentially effective techniques for the recognition of dysplastic mucosa in BE.⁵⁰ Chromoendoscopy signifies the spraying of a colored dye on the mucosal surface to enhance detail. This technique, albeit inexpensive, is time-consuming, and the interpretation of the findings is subjective and operator-dependent, so that results have been variable among several studies. With magnification endoscopy, it is necessary to maintain a fixed optical distance between the tissue to be imaged and the endoscope; the constant motion of the esophagus usually makes this difficult. Additionally, the area of mucosa visualized in each magnified image is tiny, thereby making magnification endoscopy less suitable for surveillance of long segments of Barrett's epithelium. Other barriers to the widespread application of chro-

moendoscopy and magnification endoscopy are increased procedure time and lack of reimbursement.⁵¹

In the present study, semi-automatic segmentation that involved some manual applications was used to extract an ROI. This would be unsuitable for a CAD surveillance protocol. A protocol that automatically removes artifacts and extracts the ROI would be important for high throughput applications. The CSAC method can only capture single-scale texture features. Multiple-scale methods such as the wavelet transform to decompose the image and fractal dimensional analysis may be well suited for EOCT feature extraction because they can provide multiple image scale information instead of single-scale texture features, as in the present work. In the current study, the whole ROI was used to extract texture features. However, it might be feasible to segment the dysplastic and the nondysplastic tissue region, which might substantially improve the accuracy of image classification. Only a single feature was used as a classifier in the present study. Multivariate data analysis, such as neural network and classification trees, using more image texture features may improve the classification accuracy of CAD and allow further stratification of low-grade dysplasia, high-grade dysplasia, and cancer. The current study is limited by the relatively small sample size (106); a larger study would provide more generalizable results. Refinements in EOCT instrumentation that improve image resolution and sensitivity are expected to improve CAD results and reliability.

In conclusion, we have shown that CAD can classify EOCT images of dysplasia in BE with improved accuracy compared to that achieved by humans. CAD quantifies the classification, eliminating inter-observer variability, and potentially allowing further stratification. Our results do not indicate that EOCT is sufficiently sensitive to replace the standard surveillance with the included biopsies. However, the high negative predictive value indicates that EOCT could have a useful role in targeting biopsies by eliminating mucosal areas where there is no suspicion of dysplasia. CAD has the potential to enable EOCT surveillance of large areas of Barrett's mucosa for dysplasia, which is impossible with the currently available probe technology. Moreover, with further refinements, CAD could improve the accuracy of identification of dysplasia in patients with BE.

Acknowledgments

The authors acknowledge the contributions of Dr. Douglas Rowland, Dr. Yinsheng Pan, and Brian Wolf. This work was supported by National Institutes of Health (CA94304 and CA114276).

References

1. K. R. Devault, "Epidemiology and significance of Barrett's esophagus," *Dig. Dis.* **18**, 195-202 (2000).
2. R. E. Sampliner, "Updated guidelines for the diagnosis, surveillance and therapy of Barrett's esophagus," *Am. J. Gastroenterol.* **97**, 1888-1895 (2002).
3. S. J. Spechler, "Screening and surveillance for complications related to gastroesophageal reflux disease," *Am. J. Med.* **111**(Suppl), 130S-136S (2001).
4. T. R. DeMeester, "Surgical therapy for Barrett's esophagus: prevention, protection and excision," *Dis. Esophagus* **15**, 109-116 (2002).

5. J. Theisen, J. J. Nigro, T. R. DeMeester, J. H. Peters, O. L. Gastal, J. A. Hagen, M. Hashemi, and C. G. Bremnaer, "Chronology of the Barrett's metaplasia-dysplasia-carcinoma sequence," *Dis. Esophagus* **17**, 67–70 (2004).
6. J. B. O'Connor, G. W. Falk, and J. E. Richter, "The incidence of adenocarcinoma and dysplasia in Barrett's esophagus: Report on the Cleveland Clinic Barrett's esophagus registry," *Am. J. Gastroenterol.* **94**, 2037–2042 (1999).
7. S. J. Spchler, "Barrett's esophagus: An overrated cancer risk factor," *Gastroenterology* **119**, 587–589 (2000).
8. M. Skacel, R. E. Petras, T. L. Gramlich, J. E. Sigel, J. E. Richter, and J. R. Goldblum, "The diagnosis of low-grade dysplasia in Barrett's esophagus and its implications for disease progression," *Am. J. Gastroenterol.* **95**, 3383–3387 (2000).
9. D. Hurschler, J. Borovicka, J. Neuweiler, C. Oehlschlegel, M. Sagmeister, C. Meyenberger, and U. Schmid, "Increased detection rates for Barrett's oesophagus without rise incidence of oesophageal adenocarcinoma," *Swiss Med. Wkly.* **133**, 507–514 (2003).
10. G. W. Falk, T. W. Rice, J. R. Goldblum, and J. E. Richter, "Jumbo biopsy forceps protocol still misses unsuspected cancer in Barrett's esophagus with high-grade dysplasia," *Gastrointest. Endosc.* **49**, 170–176 (1999).
11. A. B. West, M. Traube, S. Spechler, J. Goldblum, H. W. Boyce, and M. Robert, "Can therapy and surveillance prevent cancer of the esophagus?," *J. Clin. Gastroenterol.* **36**(5), S26–28 (2003).
12. H. Mashimo, M. S. Wagh, and R. K. Goyal, "Surveillance and screening for Barrett's esophagus and adenocarcinoma," *J. Clin. Gastroenterol.* **39**(4), S33–41 (2005).
13. G. Zaninotto, A. R. Parenti, A. Ruol, M. Costantini, S. Merigliano, and E. Ancona, "Oesophageal resection for high-grade dysplasia in Barrett's oesophagus," *Br. J. Surg.* **87**(8) 1102–1105 (2000).
14. D. Huang, E. A. Swanson, C. P. Lin, J. S. Schuman, W. G. Stinson, W. Chang, H. R. Hee, T. Flotte, K. Gregory, C. A. Puliafito, and J. G. Fujimoto, "Optical coherence tomography," *Science* **254**(5035) 1178–1181 (1991).
15. J. A. Izatt, M. D. Kulkarni, H. W. Wang, K. Kobayashi, and M. V. Sivak, Jr., "Optical coherence tomography and microscopy in gastrointestinal tissues," *IEEE J. Sel. Top. Quantum Electron.* **2**(1017) 1017–1028 (1996).
16. A. M. Rollins, R. Ung-arunyawee, A. Chak, R. C. K. Wong, K. Kobayashi, M. V. Sivak, Jr., and J. A. Izatt, "Real-time *in vivo* imaging of human gastrointestinal ultrastructure by use of endoscopic optical coherence tomography with a novel efficient interferometer design," *Opt. Lett.* **24**(19), 1358–1360 (1999).
17. G. J. Tearney, M. E. Brezinski, B. E. Bouma, S. A. Boppart, C. Pitris, J. F. Southern, and J. G. Fujimoto, "*In vivo* endoscopic optical biopsy with optical coherence tomography," *Science* **276**, 2037–2039 (1997).
18. B. E. Bouma, G. J. Tearney, C. C. Compton, and N. S. Nishioka, "High-resolution imaging of the human esophagus and stomach *in vivo* using optical coherence tomography," *Gastrointest. Endosc.* **51**(4), 467–474 (2000).
19. F. I. Feldchtein, G. V. Gelikonov, V. M. Gelikonov, R. V. Kuranov, and A. M. Sergeev, "Endoscopic applications of optical coherence tomography," *Opt. Express* **3**(6), 257–270 (1998).
20. G. Zuccaro, N. Gladkova, J. Vargo, F. Feldchtein, E. Zagaynova, D. Conwell, G. Falk, J. Goldblum, J. Dumot, J. Ponsky, G. Gelikonov, B. Davros, E. Donchenko, and J. Richter, "Optical coherence tomography of the esophagus and proximal stomach in health and disease," *Am. J. Gastroenterol.* **96**(9), 2633–2639 (2001).
21. P. R. Pfau, M. V. Sivak Jr., A. Chak, M. Kinnard, R. C. Wong, G. A. Isenberg, J. A. Izatt, A. M. Rollins, and V. Westphal, "Criteria for the diagnosis of dysplasia by endoscopic optical coherence tomography," *Gastrointest. Endosc.* **58**(2), 196–202 (2003).
22. V. Westphal, A. M. Rollins, E. J. Willis, M. V. Sivak Jr., and J. A. Izatt, "Correlation of endoscopic optical coherence tomography with histology in the lower GI tract," *Gastrointest. Endosc.* **61**(4), 537–546 (2005).
23. A. Das, M. V. Sivak Jr., A. Chak, R. C. K. Wong, V. Westphal, A. M. Rollins, J. Izatt, G. A. Isenberg, and J. Willis, "Role of high-resolution endoscopic imaging using optical coherence tomography (OCT) in patients with Barrett's esophagus (BE)," *Gastrointest. Endosc.* **51**(4), AB93, Part 92 (2000).
24. X. D. Li, S. A. Boppart, J. Van Dam, H. Mashimo, M. Mutinga, W. Drexler, M. Klein, C. Pitris, M. L. Krinsky, M. E. Brezinski, and J. G. Fujimoto, "Optical coherence tomography: Advanced technology for the endoscopic imaging of Barrett's esophagus," *Endoscopy* **32**, 921–930 (2000).
25. G. A. Isenberg, M. V. Sivak Jr., A. Chak, R. C. K. Wong, J. Willis, B. Wolf, D. Rowland, A. Das, and A. M. Rollins, "Accuracy of endoscopic optical coherence tomography (EOCT) in the detection of dysplasia in Barrett's esophagus," *Gastrointest. Endosc.* **62**(6), 825–831 (2005).
26. A. Das, M. V. Sivak Jr., A. Chak, R. C. K. Wong, V. Westphal, A. M. Rollins, J. Willis, G. Isenberg, and J. A. Izatt, "High resolution endoscopic imaging of the GI tract: a comparative study of optical coherence tomography versus high frequency catheter probe EUS," *Gastrointest. Endosc.* **54**, 219–224 (2001).
27. G. A. Isenberg and M. V. Sivak Jr., "Gastrointestinal optical coherence tomography," *Tech. Gastrointestinal Endoscopy* **5**(2), 94–101 (2003).
28. A. M. Rollins, M. D. Kulkarni, S. Yazdanfar, R. Ung-arunyawee, and J. A. Izatt, "*In vivo* video rate optical coherence tomography," *Opt. Express* **3**(6) 219–229 (1998).
29. M. V. J. Sivak, K. Kobayashi, J. A. Izatt, A. M. Rollins, and R. Ung-arunyawee, "High-resolution endoscopic imaging of the GI tract using optical coherence tomography," *Gastrointest. Endosc.* **51**(4), 474–479 (2000).
30. M. L. Giger, Z. Huo, M. A. Kupinski, and C. J. Vyborny, "Computer-aided diagnosis in mammography," in *Handbook of Medical Imaging, Vol. 2: Medical Imaging Processing and Analysis*, pp. 249–272, SPIE Press, Bellingham, Wash. (1999).
31. M. L. Giger, N. Karssemeijer, and S. G. Armato, "Guest Editorial: Computer-aided diagnosis in medical imaging," *IEEE Trans. Med. Imaging* **20**(12) 1205–1208 (2001).
32. X. Qi, M. V. Sivak Jr., D. L. Wilson, and A. M. Rollins, "Computer aided diagnosis in Barrett's esophagus using endoscopic optical coherence tomography," *Proc. SPIE* **5316**, 33–40 (2004).
33. I. Pitas, *Digital Image Processing Algorithms and Applications*, John Wiley & Sons, New York (2000).
34. N. Otsu, "A threshold selection method from gray-level histograms," *IEEE Trans. Syst. Man Cybern.* **SMC-9**(1), 62–66 (1979).
35. R. C. Gonzalez and R. E. Woods, *Digital Image Processing*, Addison-Wesley, London (1992).
36. R. M. Haralick, K. Shanmugam, and I. Dinstein, "Textural features for image classification," *IEEE Trans. Syst. Man Cybern.* **SM-3**(6) 610–621 (1973).
37. K. Laws, "Rapid texture identification," *Proc. SPIE* **238**, 376–380 (1980).
38. A. Al-Janobi, "Performance evaluation of cross-diagonal texture matrix method of texture analysis," *Pattern Recogn.* **34**, 171–180 (2001).
39. M. H. Horng, Y. N. Sun, and X. Z. Lin, "Texture feature coding method for classification of liver sonography," *Comput. Med. Imaging Graph.* **26**, 33–42 (2002).
40. D. Harwood, T. Ojala, M. Pietikainen, S. Kelman, and L. Davis, "Texture classification by center-symmetric auto-correlation using Kullback discrimination of distributions," *Pattern Recogn. Lett.* **16**, 1–10 (1995).
41. I. T. Jolliffe, *Principal Component Analysis*, Springer-Verlag, New York (1986).
42. S. J. Randys and A. K. Jain, "Small sample size effects in statistical pattern recognition: Recommendations for practitioners," *IEEE Trans. Pattern Anal. Mach. Intell.* **13**(3), 252–264 (1991).
43. J. M. Ponerros, S. Brand, B. E. Bouma, G. J. Tearney, C. C. Compton, and N. S. Nishioka, "Diagnosis of specialized intestinal metaplasia by optical coherence tomography," *Gastroenterology* **120**, 7–12 (2001).
44. J. A. Evans and N. S. Nishioka, "The use of optical coherence tomography in screening and surveillance of Barrett's esophagus," *Clin. Gastroenterology and Hepatology* **3**, S8–S11 (2005).
45. S. Jackle, N. Gladkova, F. Feldchtein, A. Terenteva, B. Brand, G. Gelikonov, V. Gelikonov, A. Sergeev, A. Fritscher-Ravens, J. Freund, U. Seitz, S. Schroder, and N. Soehendra, "*In vivo* endoscopic optical coherence tomography of esophagitis, Barrett's esophagus, and adenocarcinoma of the esophagus," *Endoscopy* **32**(10), 750–755 (2000).
46. S. Brand, T. D. Wang, K. T. Schomacker, J. M. Ponerros, G. Y. Lauwers, C. C. Compton, M. C. Pedrosa, and N. S. Nishioka, "Detection of high-grade dysplasia in Barrett's esophagus by spectroscopy measurement of 5-aminolevulinic acid-induced protoporphyrin IX fluorescence," *Gastrointest. Endosc.* **56**(4), 479–487 (2002).

47. M. B. Wallace, L. T. Perelman, V. Backman, J. M. Crawford, M. Fitzmaurice, M. Seiler, K. Badizasegan, S. J. Shields, I. Itzkan, R. R. Dasari, J. V. Dam, and M. S. Feld, "Endoscopic detection of dysplasia in patients with Barrett's esophagus using light-scattering spectroscopy," *Gastroenterology* **119**, 677–682 (2000).
48. K. S. L. M. Wong, A. Molckovsky, K. K. Wang, L. J. Burgart, B. Dolenko, R. L. Somorjai, and B. C. Wilson, "Diagnostic potential of Raman spectroscopy in Barrett's esophagus," *Proc. SPIE* **5962**, 140–146 (2005).
49. I. A. Scotiniotis, M. L. Kochman, J. D. Lewis, E. E. Furth, E. F. Rosato, and G. G. Ginsberg, "Accuracy of EUS in the evaluation of Barrett's esophagus and high-grade dysplasia or intramucosal carcinoma," *Gastrointest. Endosc.* **54**, 689–696 (2001).
50. M. I. Canto, "Chromoendoscopy and magnifying endoscopy for Barrett's esophagus," *Clin. Gastroenterology and Hepatology* **3**, S12–S15 (2005).
51. H. Inoue, S. E. Kudo, and A. Shiokawa, "Novel endoscopic imaging techniques toward *in vivo* observation of living cells in the gastrointestinal tract," *Dig. Dis.* **22**, 334–337 (2004).